Since January 2020 Elsevier has created a COVID-19 resource centre with free information in English and Mandarin on the novel coronavirus COVID-19. The COVID-19 resource centre is hosted on Elsevier Connect, the company's public news and information website.

Computers in Biology and Medicine 128 (2021) 104117

Contents lists available at ScienceDirect

Computers in Biology and Medicine

journal homepage: http://www.elsevier.com/locate/compbiomed

Evaluation of acridinedione analogs as potential SARS-CoV-2 main protease inhibitors and their comparison with repurposed anti-viral drugs

Vijay Kumar Bhardwaj [a,b,c], Rahul Singh [a,b], Pralay Das [c,d], Rituraj Purohit [a,b,c,*]

[a] Structural Bioinformatics Lab, CSIR-Institute of Himalayan Bioresource Technology (CSIR-IHBT), Palampur, HP, 176061, India
[b] Biotechnology Division, CSIR-IHBT, Palampur, HP, 176061, India
[c] Academy of Scientific & Innovative Research (AcSIR), CSIR-IHBT Campus, Palampur, HP, 176061, India
[d] Natural Product Chemistry and Process Development, CSIR-Institute of Himalayan Bioresource Technology (CSIR-IHBT), Palampur, HP, India

ARTICLE INFO

Keywords:
SARS-CoV-2
COVID-19
Main protease
MM-PBSA

ABSTRACT

Background: The main protease (Mpro) of SARS-CoV-2 is involved in the processing of vital polypeptides required for viral genome replication and transcription and is one of the best-characterized targets to inhibit the progression of SARS-CoV-2 in infected individuals.
Methods: We screened a set of novel classes of acridinediones molecules to efficiently bind and inhibit the activity of the SARS-CoV-2 by targeting the Mpro. The repurposed FDA-approved antivirals were taken as standard molecules for this study. Long term (1.1 μs) MD simulations were performed to analyze the conformational space of the binding pocket of Mpro bound to the selected molecules.
Results: The molecules DSPD-2 and DSPD-6 showed more favorable MM-PBSA interaction energies and were seated more deeply inside the binding pocket of Mpro than the topmost antiviral drug (Saquinavir). Moreover, DSPD-5 also exhibited comparable binding energy to Saquinavir. The analysis of per residue contribution energy and SASA studies indicated that the molecules showed efficient binding by targeting the S1 subsite of the Mpro binding pocket.
Conclusion: The DSPD-2, DSPD-6, and DSPD-5 could be developed as potential inhibitors of SARS-CoV-2. Moreover, we suggest that targeting molecules to bind effectively to the S1 subsite could potentially increase the binding of molecules to the SARS-CoV-2 Mpro.

1. Introduction

A novel coronavirus (CoV) caused a cluster of pneumonia cases during the end of December 2019 in Wuhan city of China. The novel CoV was subsequently called the severe acute respiratory syndrome coronavirus 2 (SARS-CoV-2), and the infection caused by it was named COVID-19 by the World Health Organization [1]. The SARS-CoV-2 is a single-stranded positive-sense RNA virus containing at least six open reading frames [2,3], which belongs to the *Coronaviridae* family of viruses. The first open reading frame of the viral genome of SARS-CoV-2 encodes two polyproteins (replicase 1a and replicase 1 ab), which are responsible for the mediation of vital processes like replication and transcription [4,5]. The functional polypeptides required for replication and transcription are the end products of extensive proteolytic activity on these polyproteins. The central enzyme necessary to achieve cleavage activity is the main protease (Mpro) [6]. The Mpro, through its proteolytic activity, cleaves the polyproteins to produce non-structural polypeptides. These polypeptides are required for the production of four essential structural proteins (Envelope, Spike, Membrane, and nucleocapsid proteins), and other subsidiary proteins [7,8]. The Mpro inhibition would primarily halt the multiplication of the virus inside the host body by blocking crucial processes such as genome replication and transcription.

The Mpro of CoVs is one of the most studied and extensively explored targets for the development of specific inhibitors. The Mpro is also known as 3-Chymotrypsin-like protease (3CLpro). The Mpro exists in a catalytic homodimeric (protomer A and B) form. There are three domains in each protomer. The domain I (chymotrypsin) and II (picornavirus 3 C protease-like) are the catalytic domains containing a catalytic dyad formed by residues Cys145 and His41. The domains I and II consist of six-stranded anti-parallel β-barrel structures, while the domain III is made up of five α-helices forming an anti-parallel globular cluster [9].

* Corresponding author. Structural Bioinformatics Lab, CSIR-Institute of Himalayan Bioresource Technology (CSIR-IHBT), Palampur, HP, 176061, India.
E-mail addresses: rituraj@ihbt.res.in, riturajpurohit@gmail.com (R. Purohit).

https://doi.org/10.1016/j.compbiomed.2020.104117
Received 21 September 2020; Received in revised form 1 November 2020; Accepted 7 November 2020
Available online 12 November 2020

The domain III regulates the assembly of the physiologically active dimeric form of Mpro by allowing salt bridge interactions between Glu290 and Arg4 of each protomer. The substrate-binding site is present in a crevice between domains I and II. The binding pocket consists of four subsites (S1, S1', S2, and S4) formed by the neighboring amino-acids [10]. The absence of Mpro homologs in human proteases qualifies it to be a suitable drug target with negligible cytotoxicity [11, 12].

Drug re-purposing is a non-specific and short term approach to identify potential treatment strategies to cure COVID-19 patients [13]. Many studies have suggested the use of anti-HIV and anti-HCV drugs for the treatment of COVID-19 [13–16]. However, no specific drug is yet approved for treating COVID-19 patients. The urgent demand for the development of efficient and potent drugs against SARS-CoV-2 necessities the use of *in-silico* tools for the rapid screening of potential lead molecules. Many computational studies have suggested potential inhibitors of different origins against different target proteins of SARS-CoV-2 [17–20].

A wide range of natural products has allowed enormous resources of information for basic sciences and drug discovery for pharmaceutical industries [21,22]. A systemic approach led by the experience and inspirations of many researchers have played a decisive role in successful target identification, and a rapid progression in genomics and proteomics have made this grueling task possible [23–25]. Computational strategies could be employed to screen potential targets in a stipulated time. The most probable target predicted by *in-silico* approaches could easily be tested in *in-vitro* or *in-vivo* conditions [26]. In this study, we screened a set of DSPD molecules along with repurposed FDA approved anti-HIV (Atazanavir, Indinavir, and Saquinavir), and anti-HCV (Ciluprevir and Glecaprevir) to target the SARS-CoV-2 Mpro. The selected DSPD molecules (DSPD-1 to 6) were compared on different computational parameters (Docking energy, RMSD, protein-ligand interactions, MM-PBSA binding energy, Contribution energy, and SASA) to repurposed FDA approved antiviral drugs. The central objective of the computational approach was to identify and compare the potential of DSPD molecules with repurposed antiviral drugs to inhibit the SARS-CoV-2 Mpro.

2. Materials and methods

2.1. Data sets

The x-ray crystallographic structure having 1.95 Å resolution of the Mpro of SARS-CoV-2 (PDB ID: 6Y2F) was fetched from the Protein Data

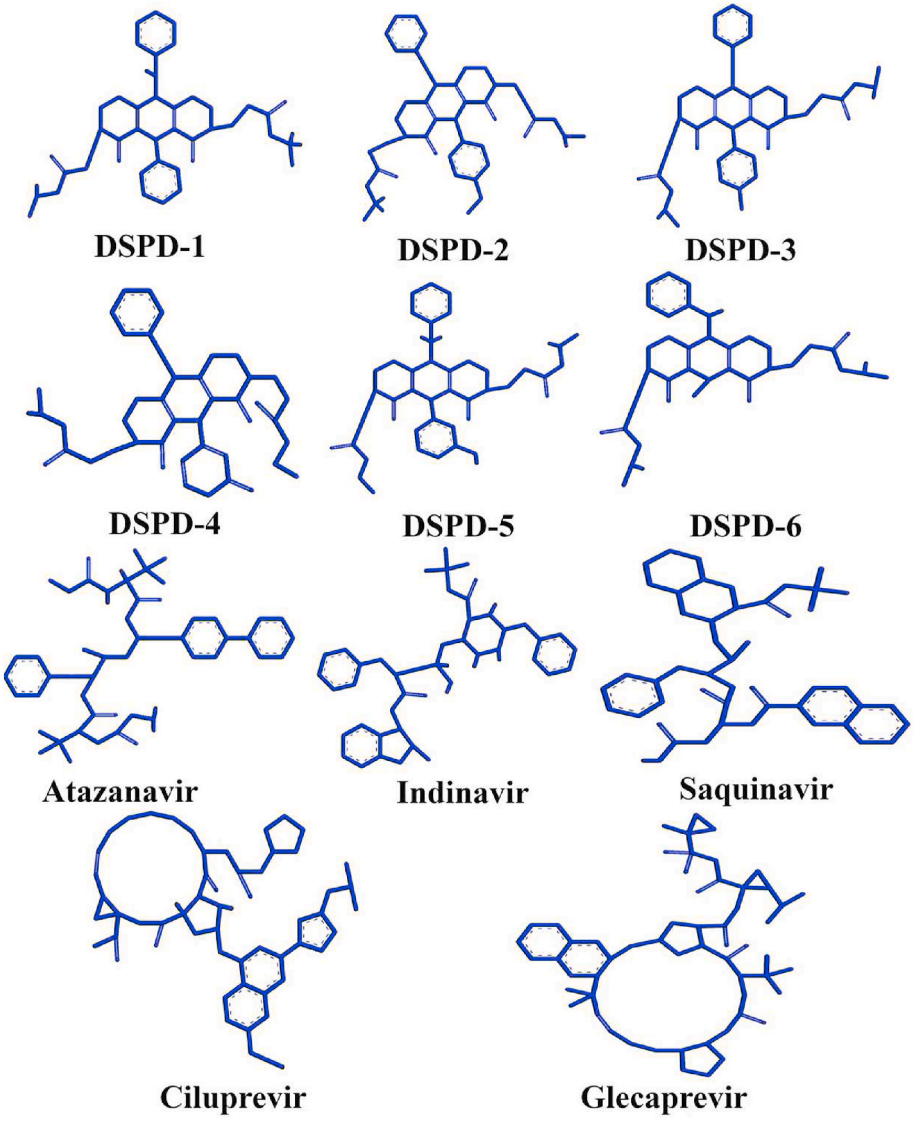

Fig. 1. 2D representations of the selected molecules for MD simulations.

Bank [14], and a cluster of FDA approved anti-HIV and anti-HCV drugs, and previously synthesized DSPD molecules were selected for the study. The protein structure was subjected to initial preparation by the "prepare protein" Wizard of the Discovery studio package [27]. The FDA approved anti-HIV drug molecules Atazanavir, Saquinavir, Indinavir, and anti-HCV Ciluprevir, Glecaprevir, were recovered from PubChem. The Gaussian16 optimized ligand geometry of every molecule was minimized by DFT protocols [28]. The molecules proposed under this study as ligand DSPD-1 to 6 have been published in our earlier report [29]. Novel classes of acridinediones (DSPD-1-6) have been synthesized under this study following microwave assisted solvent free silica mediated green approaches from ethyl-3-(2,4-dioxocyclohexyl) propanoate [30] and different amines through *in situ* formation of β-enaminoester. The diester functionality in ligand DSPD-1-6 is rare and gives a vast opportunity to outspread binding capacity and may be responsible for its best performance. The 2D representations of the selected molecules for MD simulations are shown in Fig. 1. Further to enhance the solubility of ligand DSPD-1 to 6 in hydrophilic or polar solvents, its acid salts also have been proposed under this study.

2.2. ADMET and TOPKAT predictions

The Discovery studio was used to access the drug likeliness properties and potential toxicity of novel molecules. The inbuilt published tools (ADMET and Toxicity Prediction by Komputer Assisted Technology (TOPKAT) module) and models such as the CYP2D6 Prediction, Hepatotoxic Prediction, PPB Prediction, Solubility Level, Absorption Level, 2D Polar Surface Area, AlogP98, Rat Female NTP Prediction, Rat Male NTP Prediction, Carcinogenic Potency TD50 Rat, Rat Oral LD50, Ames Prediction, DTP Prediction, Skin Irritant, and Skin Sensitization in the discovery studio package were used to calculate and analyze the pharmacokinetic profiles of DSPD molecules along with the selected FDA approved drugs [31,32].

2.3. Molecular docking

The CDOCKER docking was performed in Discovery Studio to evaluate the binding poses of the selected ligands within the active site of SARS-CoV-2 Mpro. A CHARMm (Chemistry at Harvard Macromolecular Mechanics energy) [33] based docking mechanism is employed to execute the CDOCKER docking protocol. The receptor site is maintained to be rigid, while the ligand was permitted to move freely throughout the docking protocol. The high-temperature kinetics applied to examine the flexible conformation area clutched by the molecules. The input site sphere dimensions for the ligand receptor interactions were set to 10.959, −0.514, 20.8275, 12. The number of starting random conformations and the number of rotated ligand orientations to refine for each of the conformations for 1000 dynamics steps were set to ten. Moreover, for annealing refinement, the number of heating steps were 2000 while the number of cooling sets were set to 5000. The docking parameter values of CDOCKER were kept at default. For all complexes, the ligand-binding affinity was evaluated by applying the CHARMm force field with the interaction energy. The binding pocket of the Mpro of SARS-CoV-2 was assigned as the areas within a radius of 10 Å from the center of the selected ligands. Based on the interaction energy of CDOCKER, distinct conformational poses of each molecule were produced and examined.

2.4. MD-simulations

Molecular dynamics (MD) simulations were carried out using the GROMACS 5.0.6 [34–36]. For MD simulations, the selected docked complexes were selected as the starting structures. The topology of the ligands were generated by using the GlycoBioChem PRODRG2 server [37]. The "pdb2gmx" of GROMACS was used to generate topologies for the Mpro protein. The GROMOS96 43a1 force field with spc water model were used for simulations. To the complexes at this stage, the addition of H-bonds was also done. The number of water molecules added to the simulation box were 30,086, 30,081, 30,075, 30,081, 30,076, and 30,074 for complexes with molecules DSPD-1 to DSPD-6, respectively. Similarly, for complexes with Saquinavir, Atazanavir, Indinavir, Ciluprevir, and Glecaprevir, the number of water molecules added were 30,075, 30,076, 30,080, 30,074, and 30,076, respectively. For maintaining the electro-neutrality of the system, Na^+ ions were added to the simulation system using the "gmx genion" script. To complexes with DSPD-1 to DSPD-6, Atazanavir, Indinavir, and Glecaprevir, the number of Na^+ ions added were two. One Na^+ ion was added to the complex with Saquinavir, while three Na^+ ions were added to complex with Ciluprevir. Energy minimization of the selected complexes was performed by the use of the steepest descent minimization algorithm. The MD equilibrations were further carried out in two steps: (i) Integration time of 2 fs at 300 K temperature with 500 ps under NVT was the first step. (ii) In the second step, to equilibrate the size of the system, 1 ns NPT equilibration was employed at pressure 1 bar. As the backbone C-α atoms were restained but the solvent molecules were allowed to move freely in both the steps. During equilibration, the previous step ensured the adequate solvent equilibrium in the system. The equilibrated systems were then subjected to the production phase without any restrains for a period of 100 ns. To maintain the temperature at 300 K the V-rescale temperature coupling algorithm [38] was used, and the Parrinello-Rehman pressure coupling method [39] was used to maintain the pressure of the system at 1 atm. Applying the LINCS algorithm [40], all the bonds were constrained, and on the other hand, a 10 Å cut-off was set for the non-bonded interactions. To calculate the long-range electrostatic interactions, the Particle-Mesh Ewald (PME) algorithm [41] was utilized. At every 5 ps, the energies were noted after setting a 2 fs time step. By the use of the GRID method, the neighbor list was updated after every 10 steps. The analysis was done by using various GROMACS in-built scripts such as "gmx rms" of the produced trajectories for calculating the root mean square deviations (RMSD) of backbone C-α atoms, the "gmx sas" for calculation of solvent accessible surface area (SASA). Furthermore, the "g_mmpbsa" script of GROMACS was utilized to perform the MM-PBSA studies [42]. MM-PBSA is one of the most popular endpoint *in-silico* methods to calculate binding free energy. MM-PBSA is acknowledged for its effectiveness and exactness. The binding free energy computation presents a quantitative evaluation of protein-ligand interactions that accommodate to apprehend its stability. In this method, the binding energy was calculated using the following equations:

$$\Delta G_{binding} = G_{complex\ -} (G_{receptor} + G_{ligand})$$

Where, ΔGbinding = the total binding energy of the complex, Greceptor = the binding energy of the free receptor, and Gligand = unbounded ligand.

3. Results

3.1. Docking analysis

A data-set of 19 molecules (FDA-approved drugs and selected molecules) was docked against SARS-CoV-2 Mpro to obtain the molecules with the best interaction energy (Table S1). The ligand binding poses were sorted according to their -CDOCKER energy; therefore, the conformers possessing the lowest energy score (more negative) were examined for further computations. The -CDOCKER energy of molecules with the best interactions were listed in Table 1.

3.2. FDA approved drugs with SARS-CoV-2 Mpro

The docked poses possessing minimum energies (more negative) conformers of the five FDA approved drugs (Atazanavir, Saquinavir,

Table 1
Selected DSPD molecules and FDA approved drugs based on best CDOCKER interaction energy.

S. No.	Molecules	-CDOCKER interaction energy
1	DSPD-4	69.66
2	Atazanavir	64.85
3	Saquinavir	63.52
4	Glecaprevir	62.96
5	Indinavir	62.46
6	DSPD-5	59.5
7	DSPD-3	56.93
8	DSPD-2	56.12
9	Ciluprevir	53.93
10	DSPD-6	53.45
11	DSPD-1	51.93

Indinavir, Ciluprevir, and Glecaprevir) were analyzed, as shown in Fig. 2. The binding pocket of SARS-COV-2 was occupied by the drug molecules, as illustrated by the docked poses. Atazanavir binds tightly through two hydrogen bonds with residues GLU166, and ASN142, besides other interactions such as carbon-hydrogen bonds (C–H bonds) with residues ARG188, ASP187, and LEU141. Pi-alkyl interaction with residues HIS163, CYS145, MET165, HIS41, PRO168, LEU141, and one sulfur-halogen interaction with residue MET49. Residues HIS140, GLY143, SER144, HIS172, HIS164, THR25, THR26, LEU27, GLN192, CYS44, PRO52, TYR54, THR190, and GLN189 formed van der Waals interactions (VdW). The repurposed anti-HIV drug Saquinavir interacted with the binding pocket through hydrogen bonding with GLU166, SER144, CYS145, GLY143, HIS163, and PHE140, C–H bonds with MET165, PRO168, Pi-Pi stacked with HIS41, hydrophobic Pi-alkyl interactions with CYS145 and MET165. VdW interactions with residues ASN142, HIS172, HIS164, ASP187, ARG188, MET49, GLN189, LEU167, THR26, THR25, LEU27, and LEU141. Indinavir interacted with the active site of the Mpro pocket through a hydrogen bond with LEU141 and C–H bonds with residues PHE140, GLU166, ASN142, and MET165. Moreover, attractive charge interaction with GLU166, Pi-sulfur interaction with MET49, Pi-alkyl with LEU141, and VdW interactions with other residues PRO168, LEU167, GLY143, CYS145, GLN189, ARG188, VAL186, ASP187, TYR54, HIS172, HIS41, HIS164, and HIS163. The anti-HCV drug Glecaprevir interacted within the active site via hydrogen bonds with residues GLU166, GLN192, GLY143, and ASN142. C–H bonds with residues MET165, GLN189, ASP187. Hydrophobic Pi-alkyl interactions with residues HIS163, PRO168, LEU167, and one halogen interaction with residue ARG188. Residues LEU141, PHE140, HIS172, SER144, CYS145, HIS164, MET49, HIS41, TYR54, CYS44, and THR190, formed VdW interaction. Similarly, Ciluprevir (anti-HCV) interacted with the residues in the binding pocket site through C–H bonds with ASN142, MET165, and THR190, Pi-anion interaction with GLU166, Pi-alkyl interaction with MET49, alkyl interaction with HIS41, MET165 besides VdW interaction with residues GLN189, GLY170, GLN192, PRO168, LEU167, ASP187, ARG188, HIS164, CYS145, SER144, GLY143, LEU141, LEU27, THR25, and THR26. A comprehensive information about the binding site residues involved in the binding of FDA approved drugs with the Mpro of SARS-CoV-2 was shown in Table S2.

3.3. Selected molecules with SARS-CoV-2 Mpro

The docked conformations with the minimum energy pose of the six molecules (DSPD-1 to 6), along with their corresponding 3-D interactions were depicted in Fig. 3. DSPD-1 stabilized in the binding pocket of SARS-CoV-2 through a conventional hydrogen bond with residue THR190, C–H bonds with residues ASN142, THR190, GLN189, MET165, and HIS164, Amide-Pi stacked and Pi-sulfur interactions with LEU141 and CYS145, respectively. Other contacts were Pi-alkyl interactions with HIS41, PRO168, MET165, and VdW interactions with other residues LA191, LEU167, ARG188, HIS163, HIS172, PHE140, SER144, MET49, ASP187, LEU27, GLY143, and THR25. DSPD-2 interacted through hydrogen bonding with GLN189, GLU166, HIS172, and HIS163. C–H bonds with residues PHE140, GLU166, ARG188, and VAL186. Alkyl interaction with residues MET165, HIS41, MET49, and VdW interactions with residues THR190, GLN192, HIS164, CYS145, SER144, LEU141, GLY143, ASN142, CYS44, TYR54, and ASP187. DSPD-3 formed hydrogen bonds with ASN142 and GLU166, C–H bonds with VAL186, ARG188, LEU141, ASN142, Pi-sulfur with CYS145. Pi-alkyl interactions with residues HIS41, CYS145, and MET165. Residues GLY143, SER144, PHE140, HIS163, HIS172, GLN189, THR190, GLN192, ASP187, TYR54, MET49, CYS44, THR25, HIS164, LEU27, THR26 were involved in VdW interactions. DSPD-4 interacted with the binding pocket through hydrogen bonding with residues HIS41 and GLN192, C–H bonds with MET165, ARG188, GLN189, and salt bridge interaction with HIS163. Pi-alkyl interactions with residues CYS44 and MET165. Residues ASN142, GLU166, MET49, LEU167, ASP187,

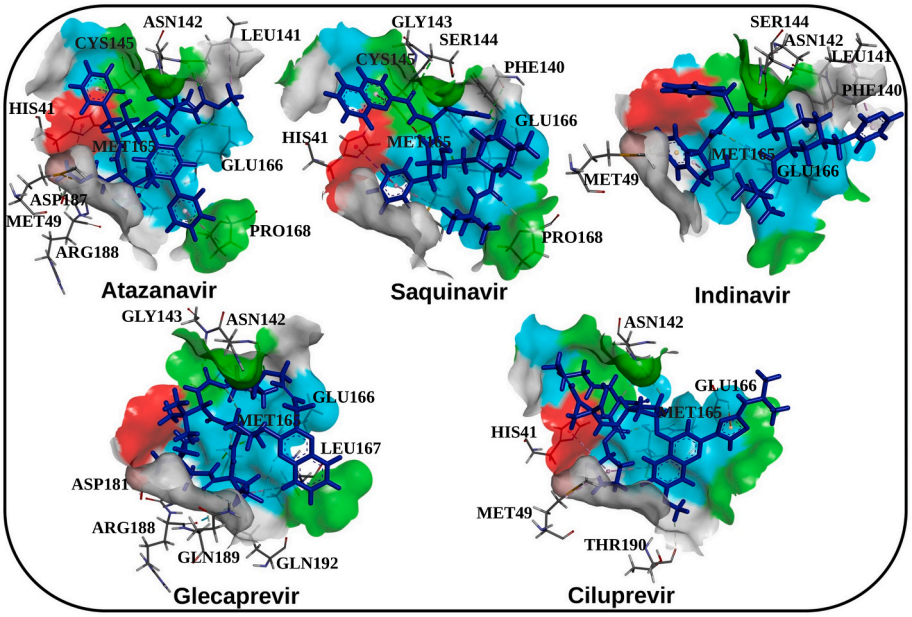

Fig. 2. 3-D binding poses of SARS-CoV-2 Mpro complexes with FDA approved drugs. The surface was colored according to the parent residues.

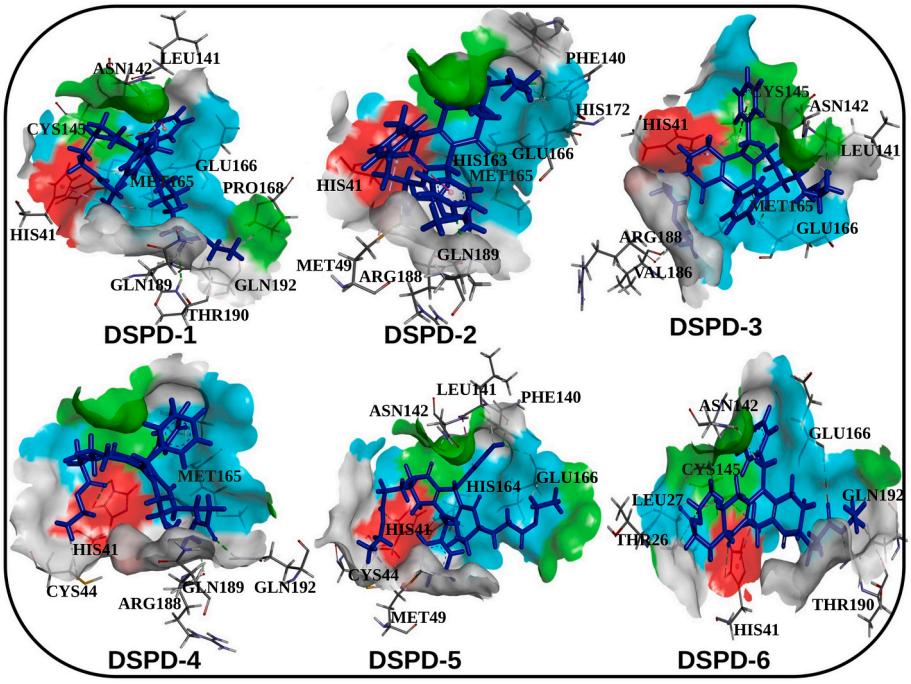

Fig. 3. 3-D binding poses of SARS-CoV-2 Mpro complexes with DSPD molecules. The surface was colored according to the parent residues.

PHE181, VAL186, HIS164, THR190, LEU141, PHE140, HIS172, GLY143, CYS145, VAL42, THR25, THR26, LEU27 formed VdW interactions. DSPD-5 stabilized in the binding pocket of SARS-CoV-2 via hydrogen bonding with residues GLU166 and PHE140. C–H bonds with residues LEU141, GLU166, ASN142, HIS164, and HIS41. Alkyl interaction with residues LEU141, CYS44, and Pi-alkyl with residue MET49, VdW interactions with residues TYR54, LEU27, CYS145, GLY143, THR25, THR45, SER144, HIS163, SER46, LEU167, PRO168, GLY170, GLN189, ASP187, ARG188, and MET165. DSPD-6 interacted through hydrogen bonding with residue GLN192 and C–H bonds with residues THR26, ASN142, HIS41, THR190. Residues LEU27, CYS145, and HIS41 formed alkyl and Pi-alkyl interactions. VdW interactions built with residues SER144, GLY143, THR25, HIS164, MET49, GLN189, PRO168, LEU167, ARG188, ASP187, GLU166, MET165, HIS163, VAL186, LEU141, HIS172, and PHE140. The overall interactions between the binding site residues of Mpro and DSPD molecules were shown in Table S3.

3.4. Toxicity and drug likeliness prediction

The ADMET properties of the DSPD molecules along with the FDA approved drugs were calculated, as summarized in Table 2. All the DSPD molecules, along with FDA approved drugs, showed no CYP2D6 inhibition. Hepatotoxic predictions were true for Atazanavir, Saquinavir, and Glecaprevir, while false for the rest of the selected molecules. Expect for Indinavir, Ciluprevir, and Glecaprevir, all the molecules were predicted to interact with plasma proteins. The highest solubility level was observed for Glecaprevir (−6.433), while the lowest was −1.598 for Indinavir among all the selected molecules. DSPD-6 and Indinavir were predicted to show good solubility, while Atazanavir, Saquinavir, Ciluprevir, and Glecaprevir showed poor solubility among all the selected molecules.

Two of the ADMET descriptors (AlogP98 and 2D polar surface area) were used to develop a 2D plot (Fig. 4). This plot was used to analyze the performance of molecules in intestinal absorption and penetration across blood brain barrier (BBB). The model included four eclipses of 99% and 95% confidence levels of BBB penetration and intestinal absorption. The results showed that DSPD-6 and Indinavir were inside eclipse of 95% confidence limit, and DSPD-4 was inside eclipse of 99% confidence limit. All other molecules were outside the eclipse of 99% confidence limit showing that these molecules were not adequate for intestinal absorption. However, the intestinal absorption could be increased by acid salts of the molecules without affecting their biological activity. The acid salts of these molecules showed good intestinal absorption (Fig. S1).

In this study, we presented the Rat Female National Toxicity Program (NTP) Prediction, Rat Male NTP Prediction, Carcinogenic potency TD50 Rat, Rat oral LD50, Ames Prediction, Developmental Toxicity

Table 2
The ADMET predictions for the DSPD molecules along with repurposed FDA approved drugs.

Name	CYP2D6 Prediction	Hepatotoxic Prediction	PPB Prediction	Solubility Level	Absorption level	AlogP98
DSPD-5	False	False	True	−5.334	2	5.57
DSPD-6	False	False	True	−5.04	0	4.78
DSPD-2	False	False	True	−5.507	2	5.79
DSPD-3	False	False	True	−6.385	2	6.56
DSPD-4	False	False	True	−4.925	1	4.86
DSPD-1	False	False	True	−5.78	2	5.81
Atazanavir	False	True	True	−5.17	3	5.69
Indinavir	False	False	False	−1.598	0	1.52
Saquinavir	False	True	True	−2.845	3	2.11
Ciluprevir	False	False	False	−7.176	3	6.07
Glecaprevir	False	True	False	−6.433	3	3.75

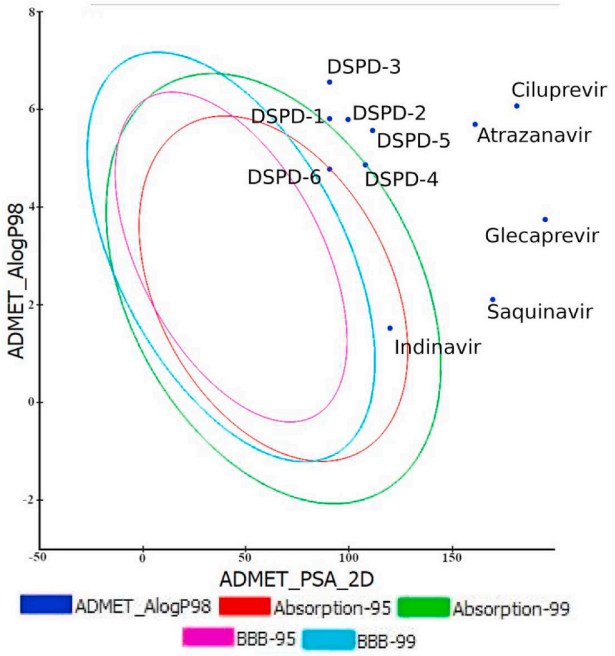

Fig. 4. 2D plot showing relationship between polar surface area and calculated AlogP98 values of the selected molecules.

Potential (DTP) Prediction, Skin Irritancy, and Skin Sensitization. The TOPKAT descriptors were summarized in Table 3. All the molecules, along with the FDA approved drugs were non-carcinogenic in rat female/male NTP predictions, non-mutagenic in Ames predictions, and non-toxic in DTP predictions. DSPD-5, DSPD-3, Saquinavir, and Ciluprevir showed no skin irritancy, while the rest of the molecules were predicted to be mildly irritant. Except for Atazanavir and Indinavir, no molecules were predicted to show skin sensitization.

3.5. Structural stability of protein-ligand complexes

The backbone C-α atoms of all the Mpro complexes having anti-HIV (Atazanavir, Indinavir, and Saquinavir), anti-HCV (Ciluprevir and Glecaprevir), and all DSPD molecules were chosen to calculate the RMSD (Fig. 5). In Mpro complexes having repurposed FDA approved drugs (Fig. 5, a), the highest average RMSD value was ~0.37 nm for Ciluprevir, while the lowest average value was observed for Indinavir (~0.32 nm). The RMSD trajectories for all the other complexes remained between these two values and converged till the end of the simulation. For Mpro complexes having DSPD molecules, the highest average RMSD was observed for DSPD-6 (~0.41 nm), while the lowest average RMSD value was ~0.31 nm for DSPD-4.

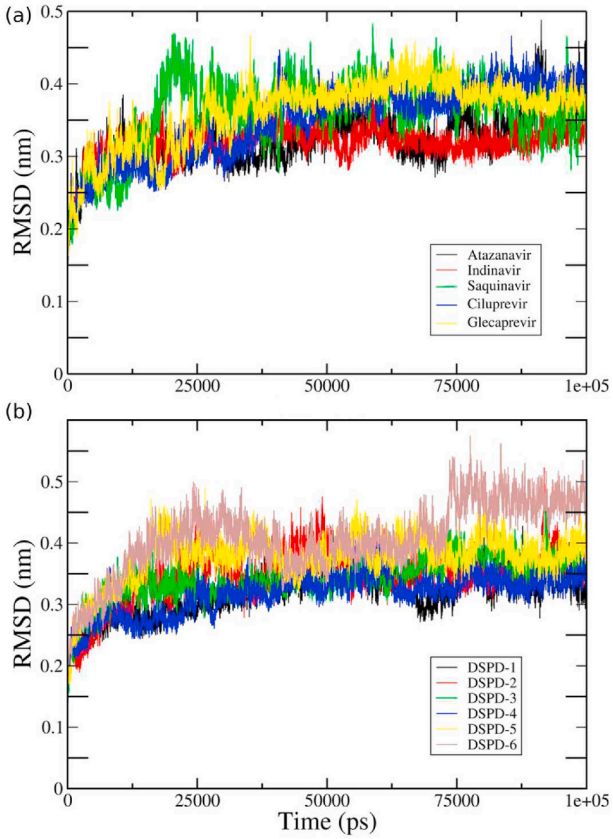

Fig. 5. RMSD of backbone C-α atoms of SARS-CoV-2 Mpro complexes with (a) FDA approved drugs and (b) DSPD molecules.

The MD simulations can be utilized to view protein-ligand interactions at different time intervals during the whole simulation run. We extracted the protein-ligand poses of the top anti-HIV (Atazanavir), anti-HCV (Glecaprevir), and top three DSPD molecules at five different time intervals (0 ns, 20 ns, 50 ns, 80 ns, and 100 ns) to visualize the position of ligands inside the binding pocket (Fig. 6). All the ligands were inside the binding pocket throughout the simulation. However, the DSPD molecules were seated more deeply inside the binding pocket as compared to Atazanavir and Glecaprevir (encircled in red for time period 0 ns). At 50 ns, DSPD-4 changed its orientation and shifted outwards (encircled in orange), matching the arrangement of Atazanavir in the binding pocket at the same time interval. DSPD-4 in further poses regained its starting pose and seemed to fit tightly inside the binding pocket for the rest of the simulation period. The binding poses of all other selected complexes were shown in Fig. S2. We also captured the snapshots of the interactions between the ligand and protein, showing

Table 3
TOPKAT results for DSPD molecules and repurposed FDA approved drugs.

Name	Rat Female NTP Prediction	Rat Male NTP Prediction	Carcinogenic potency TD50 Rat	Rat oral LD50	Ames Prediction	DTP Prediction	Skin Irritancy	Skin Sensitization
DSPD-5	Non-Carcinogen	Non-Carcinogen	50.0101	0.474043	Non-Mutagen	Non-Toxic	None	None
DSPD-6	Non-Carcinogen	Non-Carcinogen	25.5129[a]	2.14284[a]	Non-Mutagen	Non-Toxic	Mild	None
DSPD-2	Non-Carcinogen	Non-Carcinogen	3.71455	0.36639[a]	Non-Mutagen	Non-Toxic	Mild	None
DSPD-3	Non-Carcinogen	Non-Carcinogen	5.97461[a]	0.562347	Non-Mutagen	Non-Toxic	None	None
DSPD-4	Non-Carcinogen	Non-Carcinogen	5.00881[a]	0.338887[a]	Non-Mutagen	Non-Toxic	Mild	None
DSPD-1	Non-Carcinogen	Non-Carcinogen	9.61418[a]	0.89298[a]	Non-Mutagen	Non-Toxic	Mild	None
Atazanavir	Non-Carcinogen	Non-Carcinogen	0.0521036	0.966093[a]	Non-Mutagen	Non-Toxic	Mild	Weak
Indinavir	Non-Carcinogen	Non-Carcinogen	0.141855	3.53666[a]	Non-Mutagen	Non-Toxic	Mild	Weak
Saquinavir	Non-Carcinogen	Non-Carcinogen	11.1857	6.21785[a]	Non-Mutagen	Non-Toxic	None	None
Ciluprevir	Non-Carcinogen	Non-Carcinogen	0.00612124[a]	0.147204	Non-Mutagen	Non-Toxic	None	None
Glecaprevir	Non-Carcinogen	Non-Carcinogen	0.226726[a]	0.980701	Non-Mutagen	Non-Toxic	Mild	None

[a] All properties and OPS components are within expected ranges.

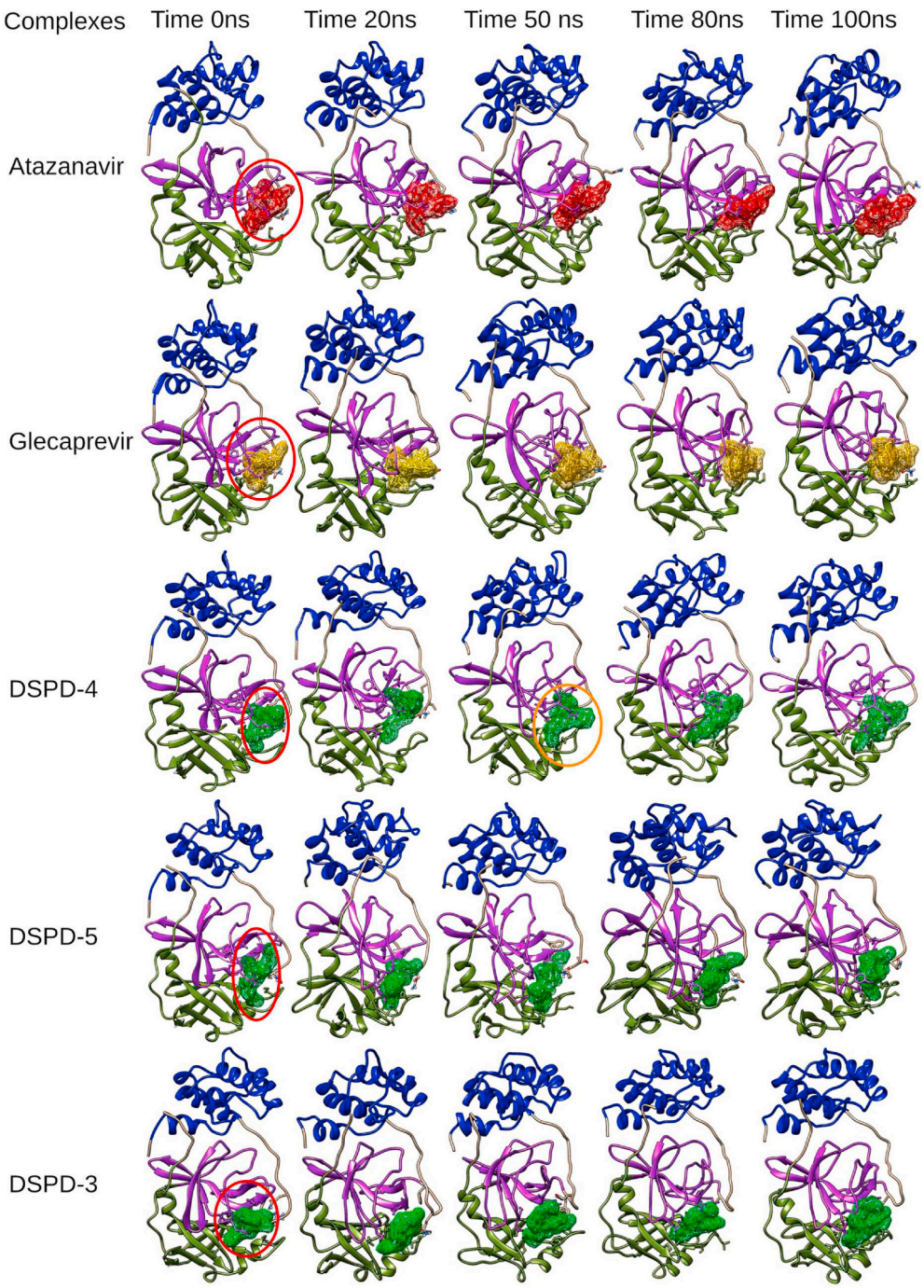

Fig. 6. Static images of selected molecules with SARS-CoV-2 Mpro complexes during MD-simulations at different time periods.

the formation of H-bonds at different time intervals during the simulations (Fig. S3). We found that all the molecules were continuously forming H-bonds with the active site residues of Mpro during the entire simulation period. Further, to validate these results, we carried out an analysis of the interaction energy between ligand and protein by the MM-PBSA method.

3.6. Interaction analysis by MM-PBSA binding energy

We calculated each component of the binding energies of Mpro with repurposed FDA-approved antiviral drugs (Atazanavir, Indinavir, Saquinavir, Ciluprevir, and Glecaprevir) and DSPD molecules (Fig. 7). The most favorable binding energy among the repurposed FDA approved drugs was shown by Saquinavir (−291.637 kJ/mol). Electrostatic and van der Waal energies contributed favorable energies of −293.960 kJ/mol and −347.024 kJ/mol, respectively. The horizontal purple line compares the overall binding energy of Saquinavir with the rest of the complexes. Two of our molecules showed more favorable binding energy than Saquinavir. The overall binding energy of the Mpro complex with DSPD-2 was −315.712 kJ/mol, while for DSPD-6, it was −299.789 kJ/mol. Moreover, the binding energy of complex with DSPD-5 (−291.534 kJ/mol) was comparable to the complex with Saquinavir. The van der Waal energy contributed most favorably for the binding of DSPD molecules to Mpro of SARS-CoV-2. The polar solvation energy contributed unfavorably to the binding of protein and ligand in all the selected complexes. In complex with Indinavir, the electrostatic energy

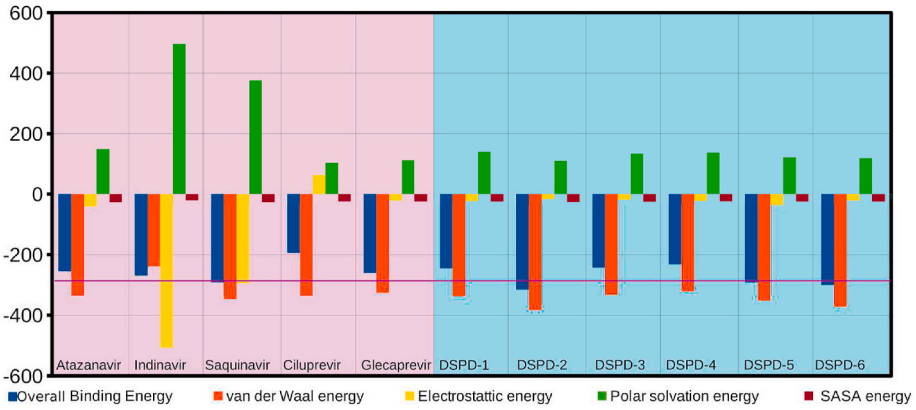

Fig. 7. MM-PBSA calculations of all components of binding free energy for all the selected complexes.

contributed more favorably (−508.56 kJ/mol) than van der Waal and SASA energy. However, the positive effect of the electrostatic energy was wiped out by higher unfavorable contributions by the polar solvation energy (513.36 kJ/mol).

We also compared the trajectories of the binding energy of the Mpro complex with Saquinavir and three topmost DSPD molecules with respect to time, as shown in Fig. 8. The binding energies with respect to the time of all the complexes were provided in Fig. S4.

The Mpro complex with DSPD-2 showed the least values of binding energy than all other complexes. The binding energy for the complex with Saquinavir increased rapidly after ~70 ns, while all other complexes followed their initial trajectories. This showed that the selected DSPD molecules exhibited firm interactions with the binding pocket of SARS-CoV-2 Mpro throughout the simulation period. Further, we decomposed the binding energy into the per residue contribution energy. The per residue energy of all the important residues contributing to the formation of the binding pocket of Mpro in complex with Saquinavir and selected DSPD molecules was compared (Fig. 9).

3.7. Exploration of binding pocket subsites

We calculated the solvent-accessible surface area (SASA) for the four subsites of the binding pocket of Mpro in complex with Saquinavir, DSPD-2, DSPD-5, and DSPD-6, as shown in Fig. 10. In the S1 subsite, the repurposed FDA-approved drug showed an average SASA value around ~5.14 nm^2, while the selected DSPD molecules 2, 5, and 6 showed ~4.21 nm^2, ~4.13 nm^2, and ~4.52 nm^2 respectively. The SASA of S1 subsite has decreased for the complexes having DSPD-2, DSPD-5, and DSPD-6 than for the complex having Saquinavir. Similarly, the SASA of S1' subsites has also reduced for the complexes having DSPD molecules when compared to complexes having Saquinavir. The SASA of subsite S2 remained unchanged for all the selected complexes. The SASA of S4 subsite was lowest for DSPD-3 (~1.07 nm^2), while the average SASA values were reported to be ~1.87 nm^2, ~2.18 nm^2, and ~2.31 nm^2 for complexes having Saquinavir, DSPD 5, and 6 respectively.

4. Discussion

In this study, we presented a computational approach to identify potential molecules that could inhibit the Mpro of SARS-CoV-2. The novel in-house synthesized acridinediones molecules, along with the FDA approved repurposed antiviral drugs, were screened for their potential to inhibit the Mpro of SARS-CoV-2. A number of recent studies have suggested potential anti-SARS-CoV-2 molecules based on computational results [17,43–45].

The structures of the DSPD molecules, along with the repurposed antiviral drugs, were subjected to energy minimization, followed by molecular docking with the Mpro of SARS-CoV-2. Molecular docking generates and ranks the receptor-ligand poses according to their interaction energies [46,47]. In all the docked complexes, the conserved residues GLU166, ASN142, CYS145, HIS41, HIS163, and GLN192, played a significant role in binding with the ligands as analyzed from the binding interaction analysis (Figs. 2 and 3). Comparing the CDOCKER energy of the selected molecules with FDA approved drugs (Table 1), we inferred that our selected molecules binding energy was best towards the ligand-binding site in the Mpro of SARS-CoV-2 and could plausibly

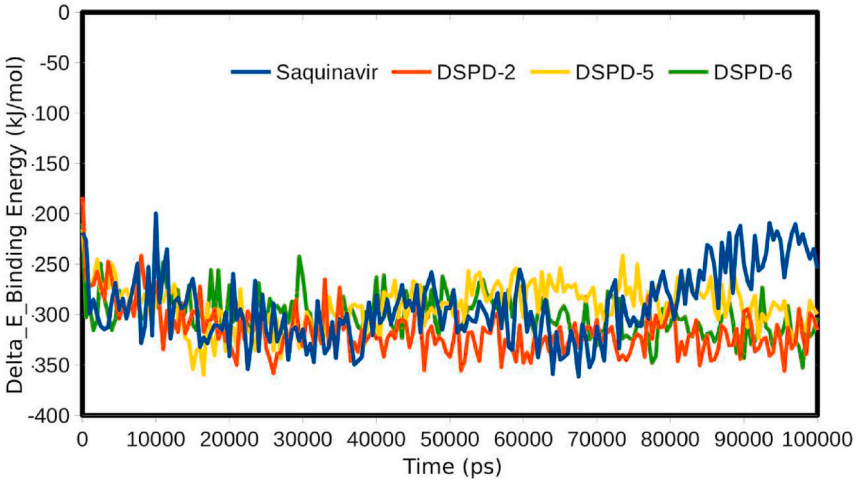

Fig. 8. Graphical representation of the Delta_E_Binding energy (kJ/mol) of Mpro complex with Saquinavir and three topmost DSPD molecules.

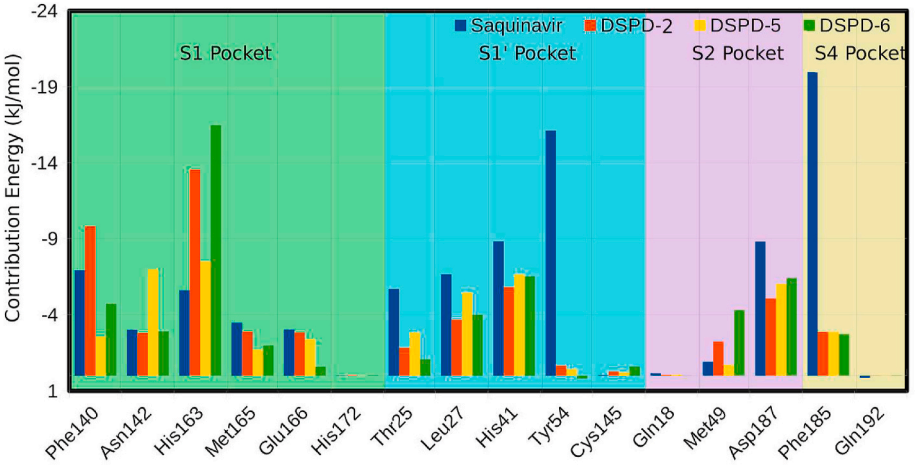

Fig. 9. Graphical representation of contribution energy of critical residues involved in the formation of Mpro binding pocket in complexes having Saquinavir and three topmost DSPD molecules.

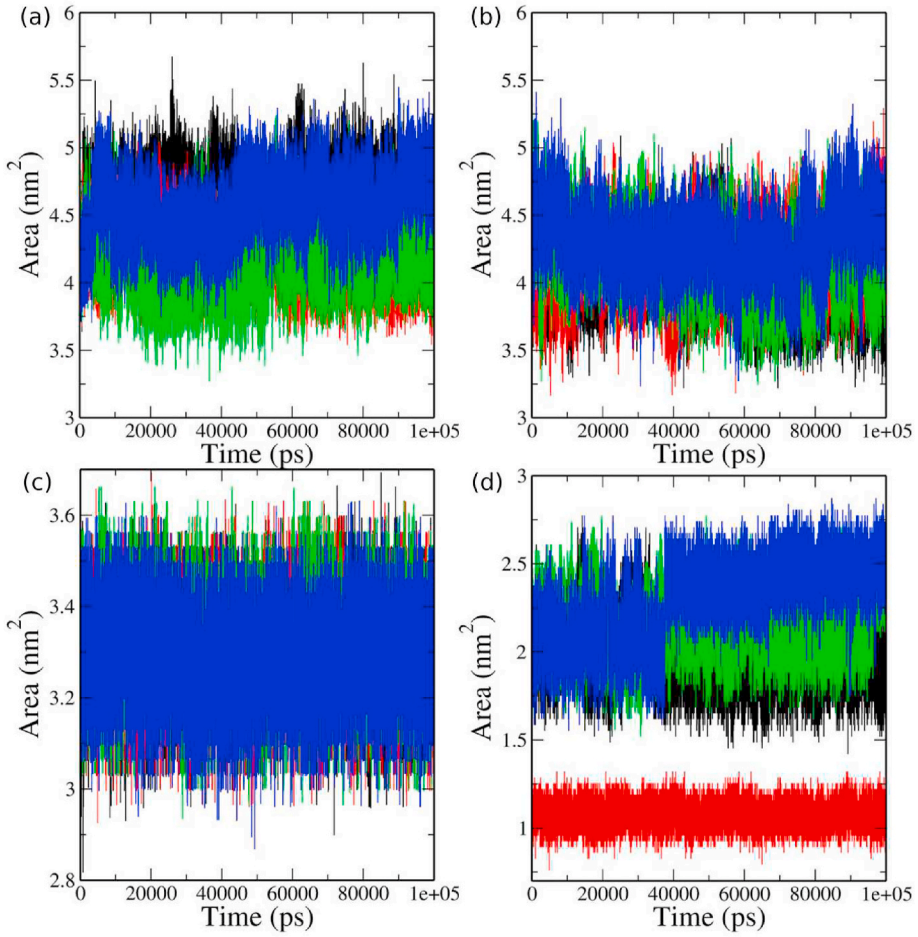

Fig. 10. The SASA plot of residues involved in the binding pocket subsites of SARS-CoV-2. (a) S1 subsite, (b) S1′ subsite, (c) S2 subsite, and (d) S4 subsite. The color representation is as follows: Saquinavir (black), DSPD-2 (red), DSPD-5 (green), and DSPD-6 (blue).

be developed as drugs for the treatment of COVID-19 patients. The docking interaction energy revealed that among the selected molecules, DSPD-4 bestowed the highest interaction energy. The selected molecules were further analyzed through MD simulations and supported by thermodynamic free energy calculations to validate the stability of the selected molecules inside the binding pocket of SARS-CoV-2 Mpro.

In order to predict the drug likeliness of DSPD molecules, we calculated the ADMET properties of these molecules along with the FDA approved drugs, as summarized in Table 2. The molecules were compared on six ADMET descriptors, such as cytochrome P450 2D6 (CYP2D6), hepatotoxicity, plasma protein binding (PPB), solubility, absorption, and AlogP98. The CYP2D6, hepatotoxicity, and PPB parameters are presented in two forms (True: inhibitor/toxic, or False: non-inhibitor/non-toxic) to evaluate their toxicity or inhibitory actions

[26]. The molar solubility of a molecule in a range between −8.0 and 0.0 is predicted by the solubility descriptor. These values are divided into five levels (−8.0 to −6.0: poor solubility, −6.0 to −4.0: low solubility, −4.0 to −2.0: optimal solubility, and −2.0 to 0.0: high solubility) [26,48]. The absorption of a molecule is predicted by the absorption level parameter of ADMET results. The absorption of a molecule is inversely proportional to the absorption level (0: good, 1: moderate, 2: low, and 3: very low) [31,48]. All the DSPD molecules passed the above parameters. However, the DSPD molecules showed lower solubility, as observed from the 2-D plot between the polar solvation area and AlogP98 values (Fig. 4). To overcome this limitation, the acid salts of the DSPD molecules could be used, which showed higher absorption, as shown in Fig. S1.

Further, the drug likeliness of the molecules was accessed by the TOPKAT tool [32,48]. TOPKAT provides both quantitative as well as qualitative predictions. The quantitative structure-activity relationship (QSTR) models are employed by the TOPKAT tool to quantitatively evaluate the toxicity. The QSTR models are then used to calculate the probability values and evaluate toxicity by optimal predictive space (OPS) [49]. The toxicity decreases with an increase in quantitative Carcinogenic potency TD50 Rat, Rat oral LD50 values, making the molecules more potent by increasing their safety index [26,31,49]. All DSPD molecules showed favorable TOPKAT results, as shown in Table 3.

The crystallographic structures are static poses of three-dimensional structures of proteins. MD simulations are employed to bring these static poses alive, providing insights into the actual protein motions in biological conditions [50–53]. The investigation of protein structure and folding simulations are dependent on various computational tools that measure structural similarity. The RMSD is a well-accepted estimator of the structural similarity of optimally aligned proteins [54]. The RMSD trajectories of all the protein-ligand complexes converged below 0.5 nm (Fig. 5). The subtle differences in the values of RMSD and the converged trajectories revealed that the simulation complexes were conformationally stable and equipotential to actual crystallographic protein structures. The conformations obtained from MD simulations were structurally stable and ideal for further computational analysis.

The protein-ligand trajectories of the well-equilateral structures were extracted at different time intervals to visualize the interaction throughout the simulation period. The DSPD molecules were seated deep inside the binding pocket throughout the simulation time. However, Atazanavir and Glecaprevir were present on the edge of the binding pocket (Fig. 6). These findings were additionally confirmed by determining the thermodynamic free energy calculations by the MM-PBSA method [42]. In the process of bond formation or protein and ligand association, energy is released and is described in the form of binding energy [55]. A negative correlation is observed between binding energy and the affinity between protein and ligand. The binding of a protein and ligand is inversely proportional to the total binding energy. The constituents of the total binding energy are polar solvation, van der Wall, SASA, and electrostatic energy [42].

Our MM-PBSA calculations showed that the FDA approved drug Saquinavir showed the most favorable energy among other selected antiviral drugs with the active site of Mpro. However, two of the in-house synthesized molecules (DSPD-2 and DSPD-6) showed better interaction energies than Saquinavir (Figs. 7 and 8). Moreover, the molecule DSPD-5 showed comparable energy with Saquinavir. Further, to get an in-depth insight into the contribution of each residue to the protein-ligand binding, we decomposed the binding free energy into per residue contribution energy [42,56].

The binding pocket of Mpro is formed by four subsites (S1, S1', S2, and S4) [10]. The S1 subsite residues (Phe140, Asn142, His163, and His172) of Mpro in complex with the selected DSPD molecules showed more favorable contribution energy than Saquinavir. In the S1 subsite, residues (Thr25 and Tyr54) of Mpro in complex with Saquinavir showed most high differences in favorable contribution energy than residues in complex with the selected DSPD molecules. Two out of three residues of the S2 pocket showed higher contribution energy in Mpro complexes having DSPD molecules than in complex with Saquinavir. However, both the residues of the S4 pocket (Phe185 and Gln192) contributed more favorably to the binding in complex with Saquinavir (Fig. 9). The results of per residue contribution energy showed that DSPD molecules could be developed as potential inhibitors for SARS-CoV-2 Mpro. The DSPD molecules interacted most favorably with the S1 subsite of Mpro binding pocket, which led to decreased binding energy (more favorable interaction). Hence, we can conclude that the molecules targeting the S1 subsite can inhibit Mpro more efficiently than ligands binding to other subsites.

In order to understand protein stability and drug design, the SASA is an important tool that quantifies the docking of ligands to proteins and packaging of residues [57]. SASA locates the exposed residues and interior seeking in a protein [27]. It is the amount of surface area available for a solvent in a biomolecule. Our analysis (Fig. 10) showed reduced SASA for subsites S1, S1', and S4 in complexes having selected DSPD molecules. These results showed that the ligand occupied most of the available area inside the subsites. These results were also supported by our ligand-protein interaction analysis, where our selected molecules were seated deep inside the binding pocket, which explained the reason for increased MM-PBSA interaction energies of residues belonging to these subsites.

5. Conclusion

COVID-19, a disease induced by SARS-CoV-2, has been the root of a global pandemic. Though extensive investigations have been published in recent days on developing effective therapeutics against this global health emergency, there is still no licensed treatment against SARS-CoV-2. The successful treatment of viral disease has proven to be a massive challenge for contemporary medicine. In the present study, acridinedione based analogs have been prioritized over repurposed anti-viral drugs. The selected DSPD molecules 2 and 6 showed better interaction energy with the binding site of SARS-CoV-2 Mpro than the topmost antiviral drug Saquinavir. These findings confirmed that the chosen molecules possessed more significant potential than the anti-viral drugs in repressing the activity of SARS-CoV-2 Mpro. Moreover, the increased binding efficiency of DSPD molecules could be attributed to higher binding with the residues of the S1 subsite of the binding pocket. The binding potential of molecules to the binding site of SARS-CoV-2 Mpro could be increased by targeting the molecules to interact more efficiently with residues of the S1 subsite of the binding pocket. To conclude, the molecules DSPD-2 and DSPD-6 could be developed as anti-SARS-CoV-2 agents to fight against the notorious virus.

Author contributions

RP conceived of and designed the study. RP, RS, VKB, and PD analyzed and interpreted the data. PD provided chemical molecules for computational studies. RP critically revised the manuscript for important intellectual content. All authors gave final approval of the version to be published.

Declaration of competing interest

The authors declare that they have no conflict of interest.

Acknowledgement

RP gratefully acknowledges the Board of Research in Nuclear Sciences, Department of Atomic Energy, Mumbai, India for financial support vide letter No: 37(1)/14/26/2015/BRNS. VB acknowledges the Department of Science and Technology, New Delhi, India for providing junior research fellowship SERB File No: ECR/2016/000031. We also acknowledge the CSIR-Institute of Himalayan Bioresource Technology,

Palampur for providing the facilities to carry out this work. This manuscript represents CSIR-IHBT communication no. 4737.

Appendix A. Supplementary data

Supplementary data to this article can be found online at https://doi.org/10.1016/j.compbiomed.2020.104117.

References

[1] A.Y. Kumar, L. Murthy, The PR of China, under its obligations for international health regulations, Int. J. Eng. Res. Technol. 9 (2020), https://doi.org/10.1101/2020.02.07.937862.

[2] Y. Chen, Q. Liu, D. Guo, Emerging coronaviruses: genome structure, replication, and pathogenesis, J. Med. Virol. 92 (4) (2020) 418–423, https://doi.org/10.1002/jmv.25681.

[3] S. Hussain, J. Pan, Y. Chen, Y. Yang, J. Xu, Y. Peng, Y. Wu, Z. Li, Y. Zhu, P. Tien, D. Guo, Identification of novel subgenomic RNAs and noncanonical transcription initiation signals of severe acute respiratory syndrome coronavirus, J. Virol. 79 (9) (2005) 5288–5295, https://doi.org/10.1128/jvi.79.9.5288-5295.2005.

[4] J. Herold, T. Raabe, B. Schelle-Prinz, S.G. Siddell, Nucleotide sequence of the human coronavirus 229e rna polymerase locus, Virology 195 (2) (1993) 680–691, https://doi.org/10.1006/viro.1993.1419.

[5] V. Thiel, J. Herold, B. Schelle, S.G. Siddell, Viral replicase gene products suffice for coronavirus discontinuous transcription, J. Virol. 75 (14) (2001) 6676–6681, https://doi.org/10.1128/jvi.75.14.6676-6681.2001.

[6] R. Hilgenfeld, From SARS to MERS: crystallographic studies on coronaviral proteases enable antiviral drug design, FEBS J. 281 (2014) 4085–4096, https://doi.org/10.1111/febs.12936.

[7] R. Ramajayam, K.P. Tan, P.H. Liang, Recent development of 3C and 3CL protease inhibitors for anti-coronavirus and anti-picornavirus drug discovery, Biochem. Soc. Trans. 39 (5) (2011) 1371–1375, https://doi.org/10.1042/BST0391371.

[8] Z. Ren, L. Yan, N. Zhang, Y. Guo, C. Yang, Z. Lou, Z. Rao, The newly emerged SARS-Like coronavirus HCoV-EMC also has an "Achilles" heel": current effective inhibitor targeting a 3C-like protease,", Protein Cell 4 (4) (2013) 248–250, https://doi.org/10.1007/s13238-013-2841-3.

[9] Z. Jin, X. Du, Y. Xu, Y. Deng, M. Liu, Y. Zhao, B. Zhang, X. Li, L. Zhang, C. Peng, Y. Duan, J. Yu, L. Wang, K. Yang, F. Liu, R. Jiang, X. Yang, T. You, X. Liu, X. Yang, F. Bai, H. Liu, X. Liu, L.W. Guddat, W. Xu, G. Xiao, C. Qin, Z. Shi, H. Jiang, Z. Rao, H. Yang, Structure of Mpro from COVID-19 virus and discovery of its inhibitors, Nature 582 (2020) 289–293, https://doi.org/10.1038/s41586-020-2223-y.

[10] H. Yang, W. Xie, X. Xue, K. Yang, J. Ma, W. Liang, Q. Zhao, Z. Zhou, D. Pei, J. Ziebuhr, R. Hilgenfeld, Y.Y. Kwok, L. Wong, G. Gao, S. Chen, Z. Chen, D. Ma, M. Bartlam, Z. Rao, Design of wide-spectrum inhibitors targeting coronavirus main proteases, PLoS Biol. 3 (10) (2005), https://doi.org/10.1371/journal.pbio.0030324.

[11] K. Anand, J. Ziebuhr, P. Wadhwani, J.R. Mesters, R. Hilgenfeld, Coronavirus main proteinase (3CLpro) Structure: basis for design of anti-SARS drugs, Science 80 (2003), https://doi.org/10.1126/science.1085658.

[12] L. Zhang, D. Lin, X. Sun, U. Curth, C. Drosten, L. Sauerhering, S. Becker, K. Rox, R. Hilgenfeld, Crystal structure of SARS-CoV-2 main protease provides a basis for design of improved α-ketoamide inhibitors, Science 80 (2020), https://doi.org/10.1126/science.abb3405.

[13] M. Wang, R. Cao, L. Zhang, X. Yang, J. Liu, M. Xu, Z. Shi, Z. Hu, W. Zhong, G. Xiao, Remdesivir and chloroquine effectively inhibit the recently emerged novel coronavirus (2019-nCoV) in vitro, Cell Res. 30 (3) (2020) 269–271, https://doi.org/10.1038/s41422-020-0282-0.

[14] B. Cao, Y. Wang, D. Wen, W. Liu, J. Wang, G. Fan, L. Ruan, B. Song, Y. Cai, M. Wei, X. Li, J. Xia, N. Chen, J. Xiang, T. Yu, T. Bai, X. Xie, L. Zhang, C. Li, Y. Yuan, H. Chen, H. Li, H. Huang, S. Tu, F. Gong, Y. Liu, Y. Wei, C. Dong, F. Zhou, X. Gu, J. Xu, Z. Liu, Y. Zhang, H. Li, L. Shang, K. Wang, K. Li, X. Zhou, X. Dong, Z. Qu, S. Lu, X. Hu, S. Ruan, S. Luo, J. Wu, L. Peng, F. Cheng, L. Pan, J. Zou, C. Jia, J. Wang, X. Liu, S. Wang, X. Wu, Q. Ge, J. He, H. Zhan, F. Qiu, L. Guo, C. Huang, T. Jaki, F.G. Hayden, P.W. Horby, D. Zhang, C. Wang, A trial of lopinavir-ritonavir in adults hospitalized with severe covid-19, N. Engl. J. Med. 382 (19) (2020) 1787–1799, https://doi.org/10.1056/NEJMoa2001282.

[15] N. Muralidharan, R. Sakthivel, D. Velmurugan, M.M. Gromiha, Computational studies of drug repurposing and synergism of lopinavir, oseltamivir and ritonavir binding with SARS-CoV-2 protease against COVID-19, J. Biomol. Struct. Dyn. (2020), https://doi.org/10.1080/07391102.2020.1752802. In press.

[16] L. Dong, S. Hu, J. Gao, Discovering drugs to treat coronavirus disease 2019 (COVID-19), Drug Discov. Ther. 14 (1) (2020) 58–60, https://doi.org/10.5582/ddt.2020.01012.

[17] V.K. Bhardwaj, R. Singh, J. Sharma, V. Rajendran, R. Purohit, S. Kumar, Identification of bioactive molecules from tea plant as SARS-CoV-2 main protease inhibitors, J. Biomol. Struct. Dyn. (2020) 1–10, https://doi.org/10.1080/07391102.2020.1766572.

[18] J.A. Jaimes, N.M. André, J.S. Chappie, J.K. Millet, G.R. Whittaker, Phylogenetic analysis and structural modeling of SARS-CoV-2 spike protein reveals an evolutionary distinct and proteolytically sensitive activation loop, J. Mol. Biol. 432 (10) (2020) 3309–3325, https://doi.org/10.1016/j.jmb.2020.04.009.

[19] E. Khodadadi, P. Maroufi, E. Khodadadi, I. Esposito, K. Ganbarov, S. Espsoito, M. Yousefi, E. Zeinalzadeh, H.S. Kafil, Study of combining virtual screening and antiviral treatments of the Sars-CoV-2 (Covid-19), Microb. Pathog. 146 (2020) 104241, https://doi.org/10.1016/j.micpath.2020.104241.

[20] J. Wang, Fast identification of possible drug treatment of coronavirus disease -19 (COVID-19) through computational drug repurposing study, J. Chem. Inf. Model. 60 (6) (2020) 3277–3286, https://doi.org/10.1021/acs.jcim.0c00179.

[21] E. Patridge, P. Gareiss, M.S. Kinch, D. Hoyer, An analysis of FDA-approved drugs: natural products and their derivatives, Drug Discov. Today 21 (2) (2016) 204–207, https://doi.org/10.1016/j.drudis.2015.01.009.

[22] N.E. Thomford, D.A. Senthebane, A. Rowe, D. Munro, P. Seele, A. Maroyi, K. Dzobo, Natural products for drug discovery in the 21st century: innovations for novel drug discovery, Int. J. Mol. Sci. 19 (6) (2018), https://doi.org/10.3390/ijms19061578.

[23] R.C. Hillig, B. Sautier, J. Schroeder, D. Moosmayer, A. Hilpmann, C.M. Stegmann, N.D. Werbeck, H. Briem, U. Boemer, J. Weiske, V. Badock, J. Mastouri, K. Petersen, G. Siemeister, J.D. Kahmann, D. Wegener, N. Böhnke, K. Eis, K. Graham, L. Wortmann, F. Von Nussbaum, B. Bader, Discovery of potent SOS1 inhibitors that block RAS activation via disruption of the RAS–SOS1 interaction, Proc. Natl. Acad. Sci. U. S. A. 116 (7) (2019) 2551–2560, https://doi.org/10.1073/pnas.1812963116.

[24] M.C. Burns, J.E. Howes, Q. Sun, A.J. Little, D.M.V. Camper, J.R. Abbott, J. Phan, T. Lee, A.G. Waterson, O.W. Rossanese, S.W. Fesik, High-throughput screening identifies small molecules that bind to the RAS:SOS:RAS complex and perturb RAS signaling, Anal. Biochem. 548 (2018) 44–52, https://doi.org/10.1016/j.ab.2018.01.025.

[25] S. Lu, H. Jang, J. Zhang, R. Nussinov, Inhibitors of ras-SOS interactions, ChemMedChem 11 (2016) 814–821, https://doi.org/10.1002/cmdc.201500481.

[26] G. Tanwar, A.G. Mazumder, V. Bhardwaj, S. Kumari, R. Bharti, Yamini, D. Singh, P. Das, R. Purohit, Target identification, screening and in vivo evaluation of pyrrolone-fused benzosuberene compounds against human epilepsy using Zebrafish model of pentylenetetrazol-induced seizures, Sci. Rep. 9 (1) (2019), https://doi.org/10.1038/s41598-019-44264-6.

[27] B. Lee, F.M. Richards, The interpretation of protein structures: estimation of static accessibility, J. Mol. Biol. 55 (3) (1971), https://doi.org/10.1016/0022-2836(71)90324-X.

[28] J. Zheng, M.J. Frisch, Efficient geometry minimization and transition structure optimization using interpolated potential energy surfaces and iteratively updated hessians, J. Chem. Theory Comput. 13 (12) (2017) 6424–6432, https://doi.org/10.1021/acs.jctc.7b00719.

[29] D. Sharma, C.B. Reddy, A.K. Shil, R.P. Saroach, P. Das, Cyclohexyl iodide promoted approach for coumarin analog synthesis using small scaffold, Mol. Divers. 17 (2013) 651–659, https://doi.org/10.1007/s11030-013-9461-y.

[30] D. Sharma, A.K. Shil, B. Singh, P. Das, Consecutive Michael-claisen process for cyclohexane-1,3-dione derivative (CDD) synthesis from unsubstituted and substituted acetone 1, Synlett 23 (2012) 1199–1204, https://doi.org/10.1055/s-0031-1290900.

[31] F. Lombardo, P.V. Desai, R. Arimoto, K.E. Desino, H. Fischer, C.E. Keefer, C. Petersson, S. Winiwarter, F. Broccatelli, In silico absorption, distribution, metabolism, excretion, and pharmacokinetics (ADME-PK): utility and best practices. An industry perspective from the international consortium for innovation through quality in pharmaceutical development, J. Med. Chem. 60 (2017) 9097–9113, https://doi.org/10.1021/acs.jmedchem.7b00487.

[32] R. Venkatapathy, C.J. Moudgal, R.M. Bruce, Assessment of the oral rat chronic lowest observed adverse effect level model in TOPKAT, a QSAR software package for toxicity prediction, J. Chem. Inf. Comput. Sci. 44 (2004) 1623–1629, https://doi.org/10.1021/ci049903s.

[33] B.R. Brooks, R.E. Bruccoleri, B.D. Olafson, D.J. States, S. Swaminathan, M. Karplus, CHARMM: a program for macromolecular energy, minimization, and dynamics calculations, J. Comput. Chem. 4 (2) (1983) 187–217, https://doi.org/10.1002/jcc.540040211.

[34] S. Páll, R. Schulz, B. Hess, J.C. Smith, T. Murtola, M.J. Abraham, E. Lindahl, GROMACS: high performance molecular simulations through multi-level parallelism from laptops to supercomputers, SoftwareX 1–2 (2015) 19–25, https://doi.org/10.1016/j.softx.2015.06.001.

[35] D. Van Der Spoel, E. Lindahl, B. Hess, G. Groenhof, A.E. Mark, H.J.C. Berendsen, GROMACS: fast, flexible, and free, J. Comput. Chem. 26 (16) (2005) 1701–1718, https://doi.org/10.1002/jcc.20291.

[36] B. Hess, C. Kutzner, D. Van Der Spoel, E. Lindahl, Grgmacs 4: algorithms for highly efficient, load-balanced, and scalable molecular simulation, J. Chem. Theory Comput. 4 (3) (2008) 435–447, https://doi.org/10.1021/ct700301q.

[37] A.W. Schüttelkopf, D.M.F. Van Aalten, PRODRG: a tool for high-throughput crystallography of protein-ligand complexes, Acta Crystallogr. Sect. D Biol. Crystallogr. 60 (8) (2004) 1355–1363, https://doi.org/10.1107/S0907444904011679.

[38] H.J.C. Berendsen, J.P.M. Postma, W.F. Van Gunsteren, A. Dinola, J.R. Haak, Molecular dynamics with coupling to an external bath, J. Chem. Phys. 81 (8) (1984) 3684–3690, https://doi.org/10.1063/1.448118.

[39] M. Parrinello, A. Rahman, Polymorphic transitions in single crystals: a new molecular dynamics method, J. Appl. Phys. 52 (1981) 7182–7190, https://doi.org/10.1063/1.328693.

[40] B. Hess, H. Bekker, H.J.C. Berendsen, J.G.E.M. Fraaije, LINCS: a linear constraint solver for molecular simulations, J. Comput. Chem. 18 (12) (1997) 1463–1472, https://doi.org/10.1002/(SICI)1096-987X(199709)18:12<1463::AID-JCC4>3.0.CO;2-H.

[41] T. Darden, D. York, L. Pedersen, Particle mesh Ewald: an N·log(N) method for Ewald sums in large systems, J. Chem. Phys. 98 (1993) 10089–10092, https://doi.org/10.1063/1.464397.

[42] R. Kumari, R. Kumar, A. Lynn, *g_mmpbsa* —a GROMACS tool for high-throughput MM-PBSA calculations, J. Chem. Inf. Model. 54 (2014) 1951–1962, https://doi.org/10.1021/ci500020m.
[43] B. Robson, Computers and viral diseases. Preliminary bioinformatics studies on the design of a synthetic vaccine and a preventative peptidomimetic antagonist against the SARS-CoV-2 (2019-nCoV, COVID-19) coronavirus, Comput. Biol. Med. 119 (2020), https://doi.org/10.1016/j.compbiomed.2020.103670.
[44] B. Robson, COVID-19 Coronavirus spike protein analysis for synthetic vaccines, a peptidomimetic antagonist, and therapeutic drugs, and analysis of a proposed achilles' heel conserved region to minimize probability of escape mutations and drug resistance, Comput. Biol. Med. 121 (2020), https://doi.org/10.1016/j.compbiomed.2020.103749.
[45] H. Iftikhar, H.N. Ali, S. Farooq, H. Naveed, S. Shahzad-ul-Hussan, Identification of potential inhibitors of three key enzymes of SARS-CoV2 using computational approach, Comput. Biol. Med. 122 (2020), https://doi.org/10.1016/j.compbiomed.2020.103848.
[46] X.-Y. Meng, H.-X. Zhang, M. Mezei, M. Cui, Molecular docking: a powerful approach for structure-based drug discovery, Curr. Comput. Aided Drug Des. 7 (2012) 146–157, https://doi.org/10.2174/157340911795677602.
[47] R. Singh, V.K. Bhardwaj, J. Sharma, P. Das, R. Purohit, Discovery and in silico evaluation of aminoarylbenzosuberene molecules as novel checkpoint kinase 1 inhibitor determinants, Genomics (2020), https://doi.org/10.1016/j.ygeno.2020.10.001. In press.
[48] B. Bhhatarai, D.M. Wilson, A.K. Parks, E.W. Carney, P.J. Spencer, Evaluation of TOPKAT, toxtree, and derek nexus in silico models for ocular irritation and development of a knowledge-based framework to improve the prediction of severe irritation, Chem. Res. Toxicol. 29 (2016) 810–822, https://doi.org/10.1021/acs.chemrestox.5b00531.
[49] N.F. Cariello, Comparison of the computer programs DEREK and TOPKAT to predict bacterial mutagenicity, Mutagenesis 17 (2002) 321–329, https://doi.org/10.1093/mutage/17.4.321.
[50] J.D. Durrant, J.A. McCammon, Molecular dynamics simulations and drug discovery, BMC Biol. 9 (2011), https://doi.org/10.1186/1741-7007-9-71.
[51] T. Hansson, C. Oostenbrink, W.F. Van Gunsteren, Molecular dynamics simulations, Curr. Opin. Struct. Biol. 12 (2) (2002) 190–196, https://doi.org/10.1016/S0959-440X(02)00308-1.
[52] V.K. Bhardwaj, R. Purohit, A new insight into protein-protein interactions and the effect of conformational alterations in PCNA, Int. J. Biol. Macromol. 148 (2020) 999–1009, https://doi.org/10.1016/j.ijbiomac.2020.01.212.
[53] V.K. Bhardwaj, R. Purohit, Structural changes induced by substitution of amino acid 129 in the coat protein of Cucumber mosaic virus, Genomics 112 (2020) 3729–3738, https://doi.org/10.1016/j.ygeno.2020.04.023.
[54] M.R. Betancourt, J. Skolnick, Universal similarity measure for comparing protein structures, Biopolymers 59 (5) (2001) 305–309, https://doi.org/10.1002/1097-0282(20011015)59:5<305::AID-BIP1027>3.0.CO;2-6.
[55] S. Nordholm, G.B. Bacskay, The basics of covalent bonding in terms of energy and dynamics, Molecules 25 (2020), https://doi.org/10.3390/molecules25112667.
[56] R. Singh, V.K. Bhardwaj, J. Sharma, R. Purohit, Identification of novel and selective agonists for ABA receptor PYL3, Plant Physiol. Biochem. 154 (2020) 387–395, https://doi.org/10.1016/j.plaphy.2020.05.005.
[57] U. Samanta, R.P. Bahadur, P. Chakrabarti, Quantifying the accessible surface area of protein residues in their local environment, Protein Eng. 15 (8) (2002) 659–667, https://doi.org/10.1093/protein/15.8.659.